Available online at www.sciencedirect.com
ScienceDirect
Journal of Hazardous Materials 158 (2008) 43–51
Journal of Hazardous Materials
www.elsevier.com/locate/jhazmat

Removal of methylene blue from aqueous solution with silica nano-sheets derived from vermiculite

Mingfei Zhao, Zhaobin Tang, Peng Liu *

State Key Laboratory of Applied Organic Chemistry and Institute of Polymer Science and Engineering, College of Chemistry and Chemical Engineering, Lanzhou University, Lanzhou, Gansu 730000, China

Received 7 September 2007; received in revised form 11 January 2008; accepted 14 January 2008
Available online 19 January 2008

Abstract

The adsorption kinetics of a cationic dye, methylene blue (MB), onto the silica nano-sheets derived from vermiculite via acid leaching was investigated in aqueous solution in a batch system with respect to contact time, initial dye concentration, pH, and temperature. Experimental results have shown that increasing initial dye concentration favors the adsorption while the acidic pH and temperature go against the adsorption. Experimental data related to the adsorption of MB on the silica nano-sheets under different conditions were applied to the pseudo-first-order equation, the pseudo-second-order equation and the intraparticle diffusion equation, and the rate constants of first-order adsorption (k_1), the rate constants of second-order adsorption (k_2) and intraparticle diffusion rate constants (k_{int}) were calculated, respectively. The experimental data fitted very well the pseudo-second-order kinetic model. The activation energy of system (E_a) was calculated as 3.42 kJ/mol. The thermodynamics parameters of activation such as Gibbs free energy, enthalpy, entropy were also evaluated and found that ΔG^*, ΔH^*, and ΔS^* are 65.95 (71.63, 77.45) kJ/mol, 0.984 (0.776, 0.568) kJ/mol, and −0.222 (−0.223, −0.224) kJ/(K mol) at 20 (45, 70) °C, respectively. The desorption of the dye on the silica nano-sheets using ethanol was also investigated primarily.

Keywords: Removal; Adsorption; Methylene blue; Silica nano-sheets; Vermiculite

1. Introduction

Many industrial processes use different synthetic chemical dyes for various purposes. Some frequent users of these chemicals include paper and pulp manufacturing, dyeing of cloth, leather treatment, printing, etc. Most of the used solutions containing such dyes are discarded as effluents. Since some of these dyes are toxic in nature, their removal from the industrial effluents is a major environmental problem [1]. Conventional methods for the removal of dyes in effluents include physical, chemical, and biological processes [2]. Physical adsorption is generally considered to be an effective method for quickly lowering the concentration of dissolved dyes in an effluent. A considerable amount of work has also been reported in the literatures regarding the adsorption of some dyes on various adsorbent surfaces such as activated carbon [3–7], silica [8–11], clay [12–18], natural polymers [19–23], synthetic polymers [24–27], waste materials [28–31], inorganic nanocomposites [32–34], MCM [35,36], various nanotubes [37–39], glass fiber [40], alumina [41], and so on.

The mica-type silicate of vermiculite possesses a layered structure. Each layer of vermiculite consists of octahedrally coordinated cations (typically Mg, Al, and Fe) sandwiched by tetrahedrally coordinated cations (typically Si and Al). The isomorphous substitution of Si^{4+} by Al^{3+} leads to a net negative surface charge that is compensated by an interlayer of exchangeable hydrated cations (Ca^{2+}, Mg^{2+}, Cu^{2+}, Na^{+}, and H^{+}) [42]. Adjoining layers are held together by a combination of electrostatic and van der Waals forces. The general chemical formula for vermiculite is $(Mg, Fe, Al)_3[(Al, Si)_4O_{10}](OH)_2M_x{\cdot}nH_2O$, where M is an exchangeable cation and x is the number of equivalents of exchangeable cations present.

The preparation of the porous silica nano-sheets via acid leaching of vermiculite was reported [43–46] and the maximum value of surface area of 672 m^2/g with total pore volume of 0.44 mL/g was achieved in the optimum leaching conditions

* Corresponding author. Tel.: +86 931 8912516; fax: +86 931 8912582.
E-mail address: pliu@lzu.edu.cn (P. Liu).

0304-3894/$ – see front matter © 2008 Elsevier B.V. All rights reserved.
doi:10.1016/j.jhazmat.2008.01.031

Table 1
Composition of the crude vermiculite (%)

SiO_2	41.20
Al_2O_3	12.68
MgO	24.22
Fe_2O_3	4.06
CaO	0.96
H_2O	3.00
Loss on ignition	6.71

[44]. It is similar to the porous silica gel. However, it is cheaper than the porous silica gel because of the abundant resources of vermiculite and the simple preparation method. So it is expected to be used as low-cost adsorbents for the treatment of the waste waters. In the present work, the adsorption properties of the porous silica nano-sheets via acid leaching of vermiculite were first investigated with the cationic dye methylene blue (MB) as target pollutant from aqueous solution as a function of stirring speed, contact time, initial dye concentration, pH and temperature. The experimental data were analyzed using pseudo-first- and second-order kinetics models, and intraparticle diffusion models.

2. Experimental

2.1. Materials

Vermiculite used was purchased from Xinjiang, China, with the composition as in Table 1. Methylene blue (MB) (CI: 52015; chemical formula: $C_{16}H_{18}ClN_3S$; molecular weight: 319.86; maximum wavelength: 662 nm) supplied by Merck, was not purified prior to use.

2.2. Silica nano-sheets

Vermiculite was pretreated with hydrochloric acid according to a reported patent [43]. To a 1-L polypropylene beaker containing 800 mL of a 2-M HCl solution was added 25 g of 250-mesh crude vermiculite at room temperature. The resulting slurry was magnetically stirred for 12 h. The product was separated by filtration and then washed thoroughly with distilled water several times until the filtrate had a pH value of 7.0. After the washing, the silica nano-sheets obtained were stored as aqueous suspension for the further use. Part of the aqueous suspension was dried and the white powder obtained was used for the analysis and characterization (Fig. 1).

2.3. Adsorption

All of the MB solution was prepared with distilled water. 10 mL silica nano-sheets suspension (including 0.23 g silica nano-sheets) was shaken with 90 mL of dye solution of known initial concentration at desired pH and temperature at 150 rpm for 180 min. The pH of the solution was adjusted with 0.1N HCl or 0.1N NaOH by using a Model 3C Digital pH-meter with a combined pH electrode. The pH-meter was standardized with NBS buffers before every measurement. A constant bath was used to keep the temperature constant. At the end of the adsorption period, the solution was centrifuged for 10 min at 15,000 rpm. After centrifugation, the dye concentration in the supernatant solution was analyzed using a UV spectrophotometer (Shimadzu UV-260) by monitoring the absorbance changes at a wavelength of maximum absorbance (662 nm). The samples were pipetted from the reaction medium by the aid of a very thin point micropipette, which prevented the transition to the solution of the silica nano-sheet samples. Preliminary experiments showed that the effect of the separation time on the amount of adsorbed dye was negligible.

The amounts of dye adsorbed on silica nano-sheets at any time, t, were calculated from the concentrations in solutions before and after adsorption. At any time, the amount of MB adsorbed (mol/g) (q_t), onto silica nano-sheets was calculated from the mass balance equation as follows:

$$q_t = \frac{V(C_0 - C_e)}{W} \quad (1)$$

where q_t is the amount of adsorbed dye on silica nano-sheets at any time (mmol/g); C_0 and C_e are the initial and equilibrium

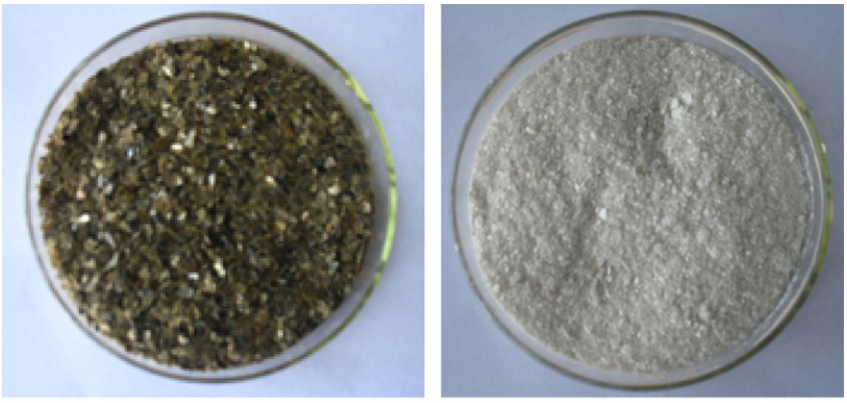

(a) vermiculite (b) silica nano-sheets

Fig. 1. Photos of (a) vermiculite and (b) silica nano-sheets.

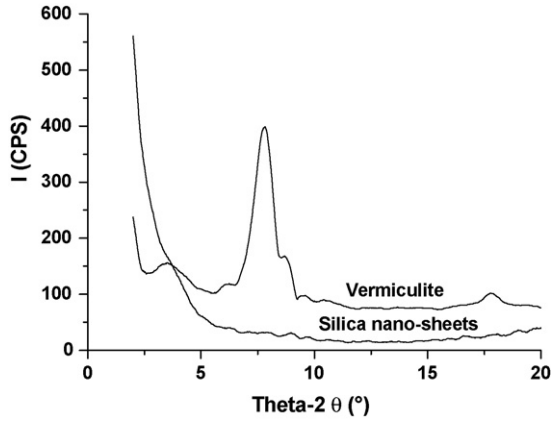

Fig. 2. X-ray diffraction of vermiculite and silica nano-sheets.

liquid-phase concentrations of MB (mmol/L), respectively; V is the volume of MB solution, and W is the mass of silica nano-sheets sample used (g) [47,48]. The Δq_t% of all the determined values was <3.0%.

2.4. Desorption

10 mL silica nano-sheets suspension (including 0.23 g silica nano-sheets) was stirred with 90 mL of dye solution at 150 rpm for 180 min. The initial dye concentration and pH were 22.39 mg/L and 5.5, respectively. At the end of the adsorption period, the solution was centrifuged for 10 min at 15,000 rpm. The dye-adsorbed silica nano-sheets were dried with IR lamp.

0.1 g of the dried product was added into 100 mL ethanol or water/ethanol solutions with certain v/v ratios with different pH values. The mixtures were stirred at 150 rpm for 60 min. Then the supernatant solutions were analyzed using UV spectrophotometer.

2.5. Analysis and characterization

The XRD patterns were recorded in the range of $2\theta = 10$–80° by step scanning with a Shimadzu XRD-6000 X-ray diffractometer. Nickel-filter Cu Kα radiation ($\lambda = 0.15418$ nm) was used with a generator voltage of 40 kV and a current of 30 mA. The morphology of the silica nano-sheets was characterized with a JEM-1200 EX/S transmission electron microscope (TEM). The silica nano-sheets suspended colloid solution was deposited on a copper grid covered with a perforated carbon film. The surface morphologies of the silica nano-sheets were characterized with a Philips XL-20 scanning electron microscope (SEM) (Philips Co., The Netherlands). The Zeta potentials of the silica nano-sheets at different pH values were determined with Zetasizer Nano ZS (Malvern Instruments Ltd., UK).

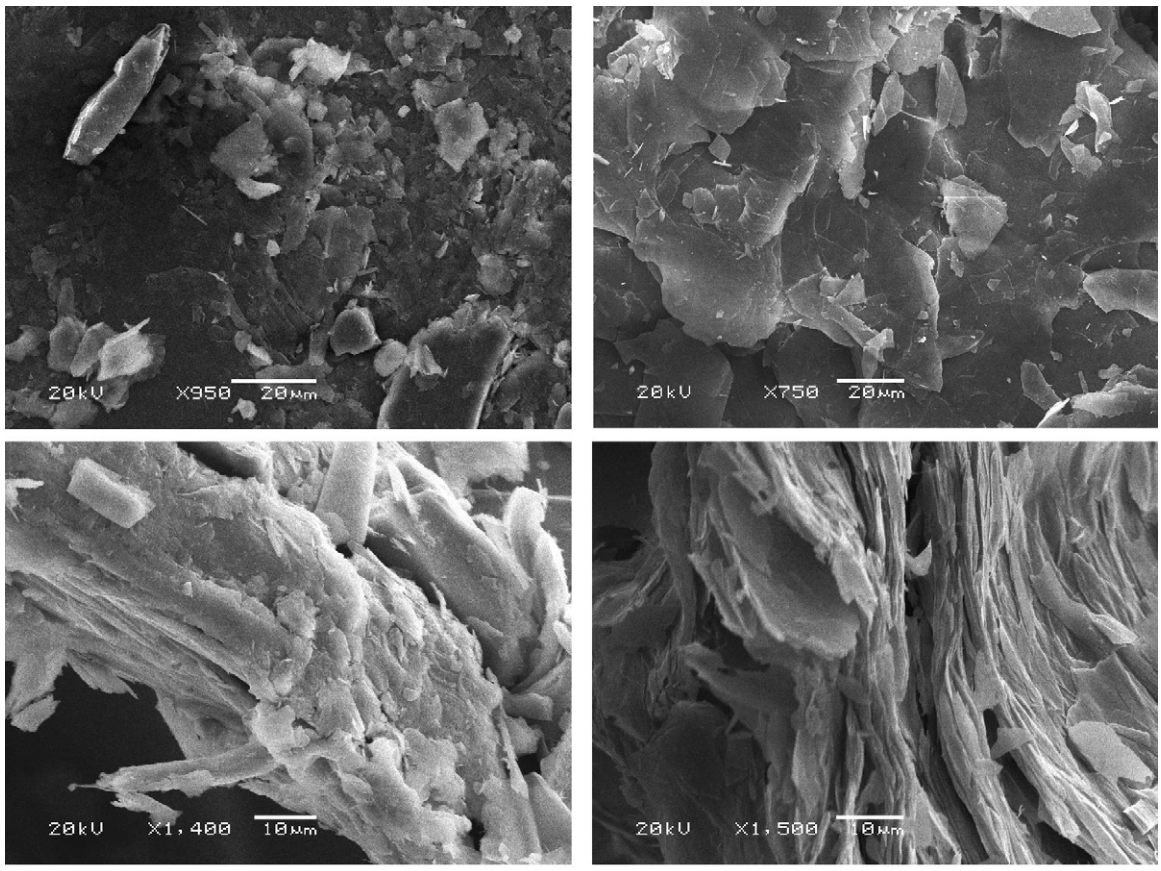

(a) vermiculite (b) silica nano-sheets

Fig. 3. SEM images.

The concentration of the dye was determined using a UV–vis recording spectrophotometer-260 (UV-260, Shimadzu Co., Japan) at an absorbance wavelength of 662 nm.

3. Results and discussion

3.1. Silica nano-sheets

Fig. 2 shows XRD of vermiculite before and after the acid treatment. The raw vermiculite yielded diffraction peaks at $2\theta = 3.5^\circ$, 7.3°, and 8.7°. The diffraction peaks at $2\theta = 7.3^\circ$ (0 0 1, $d = 1.2$ nm) represented the interlayer spacing of VMT sample while the peaks at 3.5° and 8.7° were probably resulted from the impurities within vermiculite [49,50]. After a contact time of 12 h with 2.0 M HCl, the peak corresponding to a layer gap of 1.2 nm was missing. This indicated that the silicate was delaminated and the platelets of vermiculite were less than tens cells or layers of single crystals [43]. The SEM (Fig. 3) and TEM (Fig. 4) in this work directly confirmed this, too. After being delaminated, the silica nano-sheets (Fig. 3) showed ordered layered structures compared with the pristine vermiculite. The terrace structure of the silica nano-sheets was observed by TEM (Fig. 4). The grayish region represented the mono-layered silica nano-sheets and the darker region represented the multi-layered terrace structures.

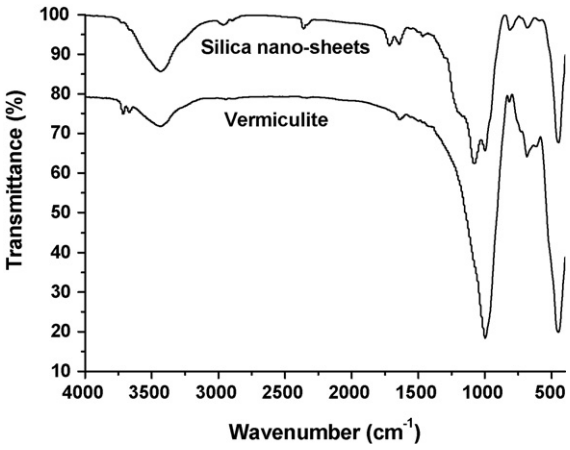

Fig. 5. FT-IR spectra of vermiculite and silica nano-sheets.

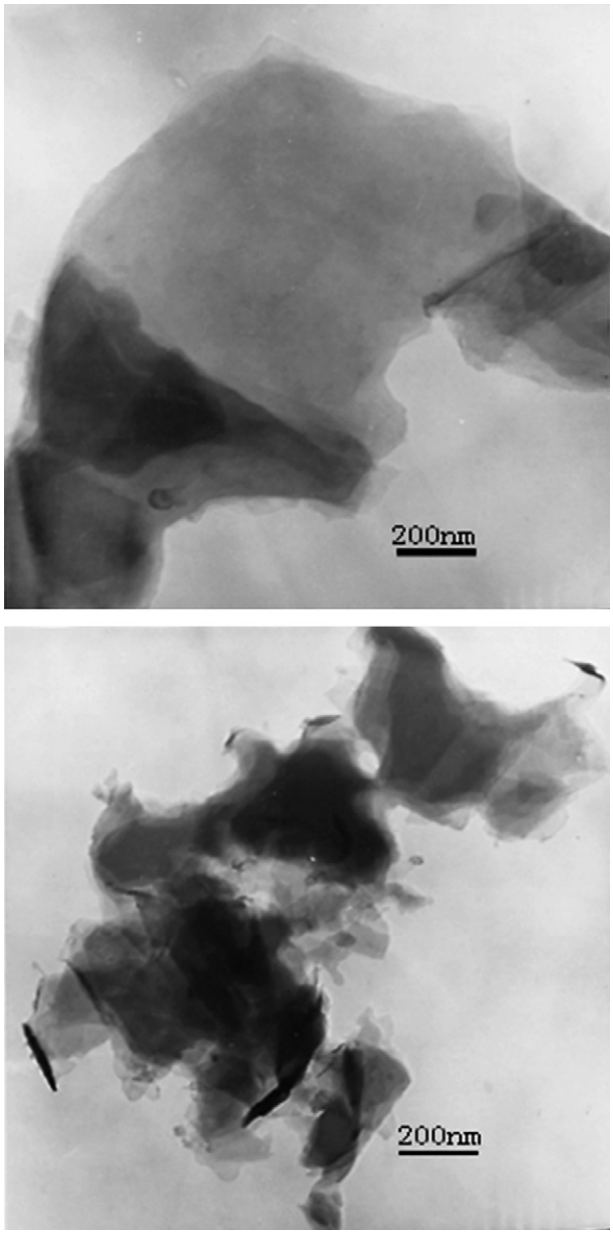

Fig. 4. TEM images of silica nano-sheets.

In the FTIR spectrum of pristine VMT (Fig. 5), the peaks at 487, 674, 813, and 1000 cm^{-1} can be ascribed to Si–O, Al–O, Al–O–H, and Si–O vibrations, respectively [51,52]. The peaks at 1635 and 3420 cm^{-1} are assigned to hydration HOH and –OH vibrations. The peak at 1440 cm^{-1} may come from the NH_4^+ cations in the interlayer of the clay [44]. As shown in Fig. 5, it is evidenced that acid treatment led to some changes in the FTIR spectrum of vermiculite. The peak corresponding to –OH groups shifted to a higher wave number (from original ~3420 to ~3439 cm^{-1}), and the peak due to Si–O at 1000 cm^{-1} also shifted to ~1090 cm^{-1}, while the Al–O vibration peak almost disappeared and Al–O–H vibration peak became sharp. The phenomena were believed to be resulted from that the acid treatment process made the hydroxyl groups within the interlayers exposed "out" (on the surface of the delaminated vermiculite sheets), and the acid treatment of vermiculite made the cleavage of some Al–O bonds of the Al–O octahedron of vermiculite and formed Al–O–H groups. In addition, the peak at 1440 cm^{-1} disappeared, indicating that NH_4^+ had been exchanged during the acid treatment.

The effects of pH value on the zeta potentials of the silica nano-sheets are illustrated in Fig. 6. In the studied pH range, the silica nano-sheets showed the negative zeta potential. This indicated that the surfaces of the silica nano-sheets were negative charged in the pH range. Continuously increasing the pH value to the basic condition, its absolute value increased. Moreover, the absolute values of the zeta potential kept <5 mV in the acidic solution. And the absolute values increased quickly with the increasing pH value in the basic solutions.

3.2. Adsorption rate

3.2.1. Effect of contact time and initial dye concentration

The initial concentration provides an important driving force to overcome all mass transfer resistances of the dye between the aqueous and solid phases. The effect of concentration on contact time was also investigated as a function of initial dye concentration. The effect of initial dye concentration and contact time on the removal rate of MB by the silica nano-sheets is shown in Fig. 7(a). As shown, the adsorption increases with increasing initial dye concentration. The removal of dye depends on the concentration of the dye. Again, adsorption increased with an increase in contact time. The equilibrium was attained at 90 min.

The amount of MB adsorbed at equilibrium increases from 6.88 to 11.77 mg/g by increasing the initial MB concentration from 15.99 to 28.79 mg/L with the adsorption condition of initial pH 7 and 20 °C. The results show that dye uptake is rapid for the first 15 min and slower and slower and finally attains saturation within about 90 min. Compared with the adsorption of MB on the pristine vermiculite (Fig. 7(b)), the silica nano-sheets had the higher adsorption capacities and the faster adsorption rate.

3.2.2. Effect of pH

Effect of pH on the removal rate of MB by the silica nano-sheets is shown in Fig. 8. As the pH increased, the removal rate decreased. The pH value of the dye solution plays an important role in the whole adsorption process and particularly on the adsorption capacity. It was found that the adsorption capacity increased with the increasing pH values in the investigated range. And the highest pH value was selected as pH 7 to avoid the breakage of the silica nano-sheets. As shown in Fig. 6, the negative charged surface revealed and the negative charge density increased with the increasing pH value. So the adsorption capacity increased with the increasing pH value.

3.2.3. Effect of temperature

Fig. 9 exhibits contact time versus adsorbed amount graph at different temperatures. The initial pH was selected as 7 in order to avoid the impossible breakage of the silica nano-sheets at higher temperatures. The equilibrium adsorption capacity of MB onto the silica nano-sheets was found to decrease with increasing temperature, decreasing from 9.38 mg/g at 20 °C to 9.32 mg/g at 70 °C indicating that the dye adsorption on the adsorbent was favored at lower temperatures. And the adsorption equilibrium was attained slowly with the higher temperature.

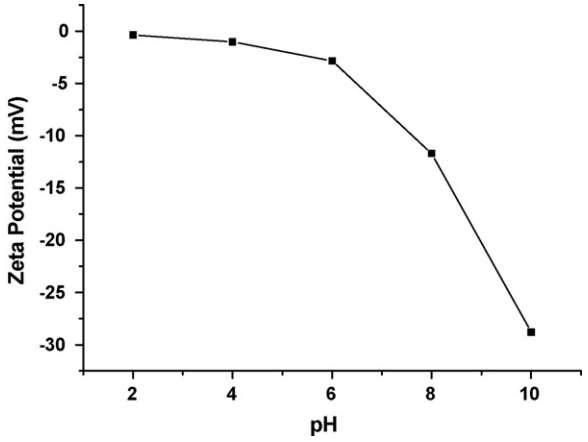

Fig. 6. Zeta potentials of the silica nano-sheets.

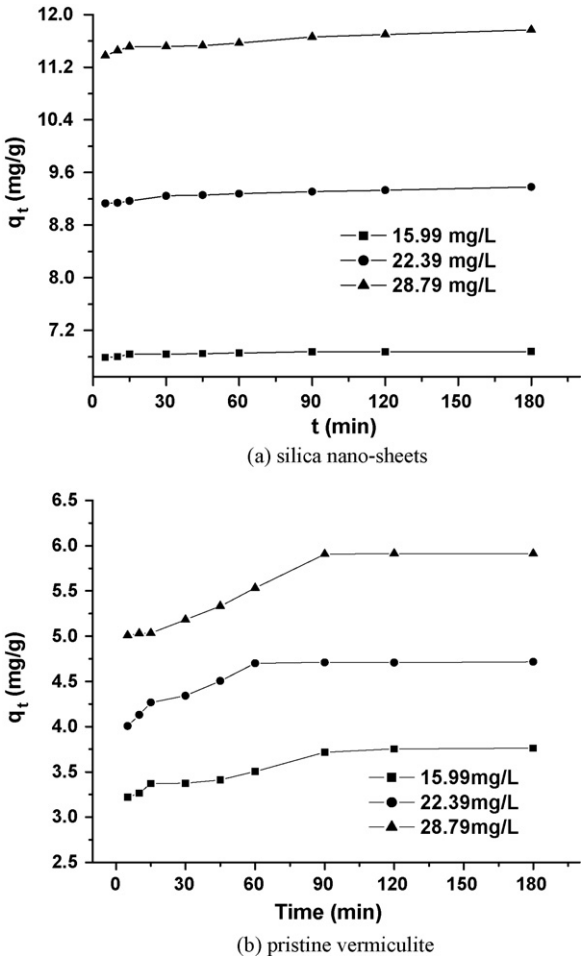

Fig. 7. Effect of contact time and initial dye concentration on adsorption of MB from aqueous solutions (20 °C, pH 5.5).

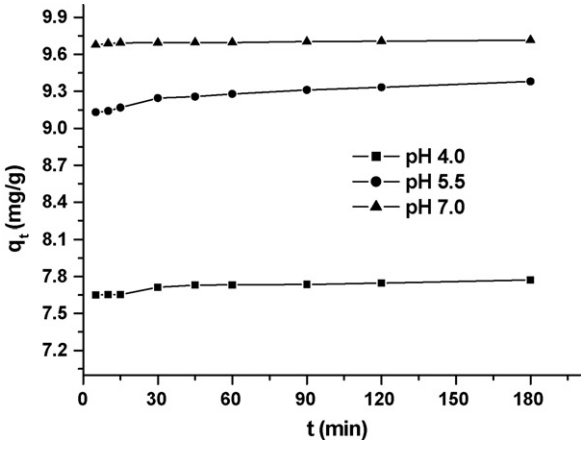

Fig. 8. Effect of contact time and initial pH on the removal rate of MB onto silica nano-sheets from aqueous solutions (20 °C, C_0: 22.39 mg/L).

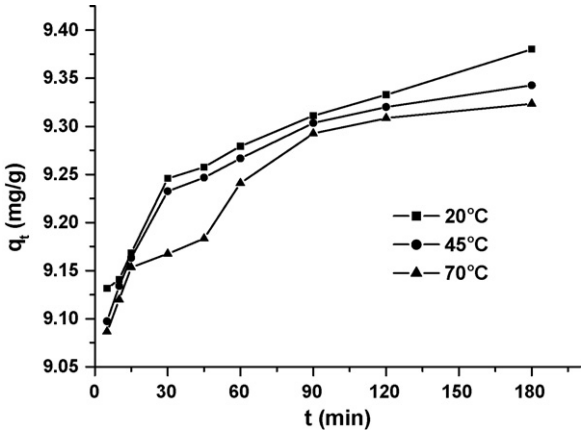

Fig. 9. Effect of contact time and temperature on the removal rate of MB onto silica nano-sheets from aqueous solutions (C_0: 22.39 mg/L, pH 5.5).

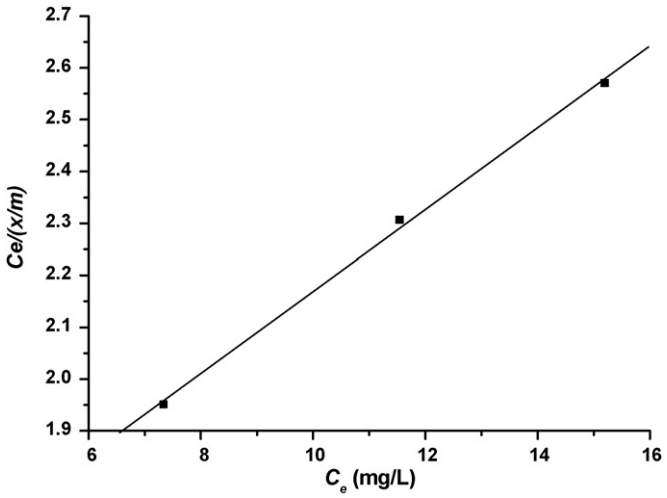

Fig. 10. Langmuir isotherm plots for the adsorption of MB on the silica nano-sheets. Contact time, 24 h; temperature, 20 °C.

3.3. Langmuir equilibrium isotherm

The Langmuir equation can be represented as follows:

$$\frac{C_e}{x/m} = \frac{1}{kb} + \frac{C_e}{b} \quad (2)$$

where C_e is the equilibrium concentration of MB remaining in the solution and x/m is the quantity of MB adsorbed per unit weight of the silica nano-sheets. The Langmuir constants are called adsorption capacity (b) and bonding energy constant (k). The Langmuir line for MB is shown in Fig. 10 (points: experimental data; line: Langmuir model). The adsorption capacity (b) and bonding energy constant (k) were found to be 12.66 mg/g and 0.057 L/mg, calculated from the Langmuir model line, respectively. The Langmuir model effectively describes the sorption data with R^2 values of 0.998. It showed that the adsorption of MB by the silica nano-sheets fits the Langmuir equilibrium isotherm perfectly.

3.4. Adsorption kinetics

3.4.1. The pseudo-first-order kinetic model

The pseudo-first-order kinetic model has been widely used to predict dye adsorption kinetics. A linear form of pseudo-first-order model was described by Taty-Costodes [53]:

$$\log(q_{eq} - q_t) = \frac{\log\ q_{eq} - k_{pf}t}{2.303} \quad (3)$$

where q_t is the amount adsorbed at time t (mg/g), and k_{pf} is the equilibrium rate constant of pseudo-first-order adsorption (min^{-1}). The values of $\log(q_{eq} - q_t)$ were calculated from the kinetic data.

The calculated q_{eq}, k_{pf}, and the corresponding linear regression correlation coefficient r_1^2 values are shown in Table 2. It was observed that the rate constant k_{pf} increased first with an increase in temperature and then decreased. It was also observed that correlation coefficients were lower for all temperatures. This shows no applicability of the pseudo-first-order model in predicting the kinetics of the MB adsorption onto the silica nano-sheets.

3.4.2. The pseudo-second-order kinetic model

The kinetic data were further analyzed using Ho's pseudo-second-order kinetics, represented in Ref. [54]:

$$\frac{t}{q_t} = \frac{1}{k_{ps}q_{eq}^2} + \frac{t}{q_{eq}} \quad (4)$$

where k_{ps} is the rate constant of second-order adsorption (g/mg min). The values were calculated from the kinetic data (Fig. 9). A plot between t/q versus t gives the value of the constants k_{ps} (g/mg min) and also q_{eq} (mg/g) can be calculated.

The curves of the plots of t/q_t versus t were given in Fig. 11 and the calculated q_{eq}, k_{ps}, and the corresponding linear regression correlation coefficient r_2^2 values are summarized in Table 2. The linear plots of t/q_t versus t show good agreement between experimental and calculated q_{eq} values. The correlation coefficients for the second-order kinetics model (r_2^2) are greater than

Table 2
Adsorption kinetic parameters of methylene blue onto silica nano-sheets

T (°C)	Pseudo-first-order			Pseudo-second-order				Intraparticle diffusion		
	k_{pf} (min^{-1})	q_e[a] (mg/g)	r_1^2	q_e[b] (mg/g)	k_{ps} (g/mg min)	q_e[a] (mg/g)	r_2^2	k_{id} (mg/g $min^{1/2}$)	C	r_3^2
20	0.014	9.38	0.967	9.38	0.248	9.38	0.999	0.023	9.09	0.981
45	0.026	9.34	0.808	9.35	0.272	9.34	0.999	0.022	9.08	0.964
70	0.024	9.32	0.967	9.34	0.305	9.32	0.999	0.022	9.05	0.976

[a] Experimental.
[b] Calculated.

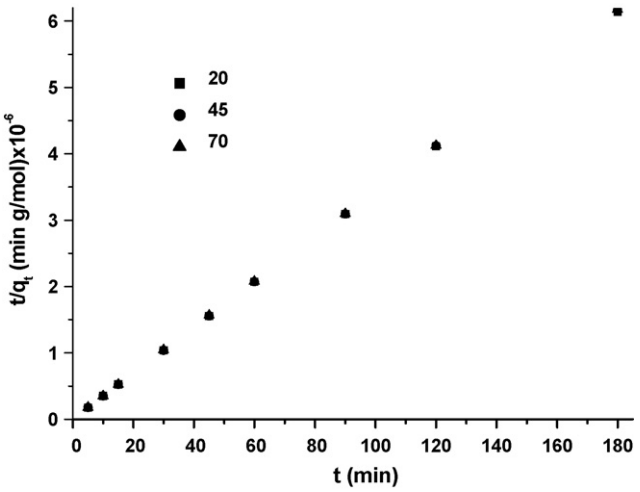

Fig. 11. Second-order kinetic equation for adsorption of MB onto silica nano-sheets at different temperatures (C_0: 0.070 mol/L, pH 5.5).

0.999, indicating the applicability of this kinetics equation and the second-order nature of the adsorption process of MB onto the silica nano-sheets.

3.4.3. Intraparticle diffusion

The adsorbate species are most probably transported from the bulk of the solution into the solid phase through an intraparticle diffusion process, which is often the rate-limiting step in many adsorption processes. The possibility of intraparticle diffusion was explored by using the intraparticle diffusion model [55]:

$$q_t = k_{id} t^{1/2} + C \quad (5)$$

where C is the intercept and k_{id} is the intraparticle diffusion rate constant (mol/g min$^{1/2}$). Plots between t/q versus t were given in Fig. 12. The values k_{id}, C, and the corresponding linear regression correlation coefficient r_3^2 values are given in Table 2. The intraparticle rate constants calculated from Fig. 12 are 0.023, 0.022, and 0.022 mg/g min$^{1/2}$ at 20, 45, and 70 °C, respectively.

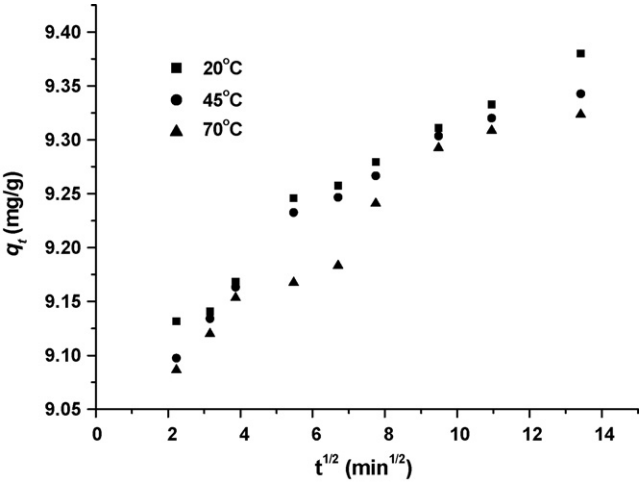

Fig. 12. Intraparticle diffusion plots for MB onto silica nano-sheets (C_0: 22.39 mg/L, pH 5.5).

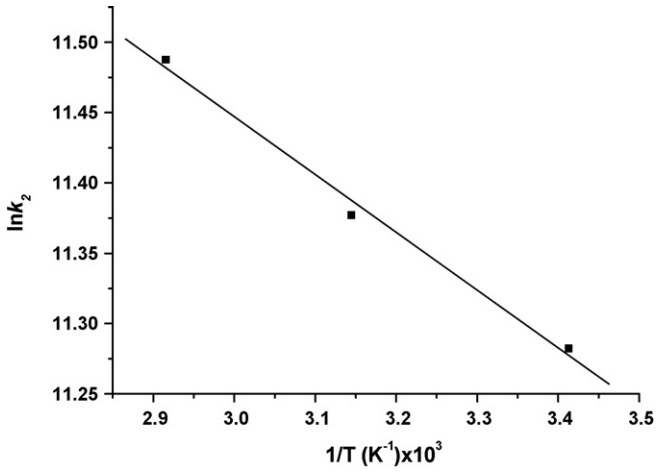

Fig. 13. Arrhenius plots for adsorption of MB (C_0: 0.070 mol/L, pH 5.5).

From Table 2, it is observed that k_{id} decreased slightly with the increasing temperature.

3.4.4. Activation of the thermodynamic parameters

The k_2 values of the second-order kinetic equation for adsorption of MB onto silica nano-sheets at different temperatures (C_0: 0.070 mol/L (22.39 mg/L), pH 5.5) were calculated to be 7.94×10^4 (20 °C), 8.73×10^4 (45 °C), and 9.75×10^4 g/(mol min) (70 °C), from the data in Fig. 13, respectively. The thermodynamic parameters including the Arrhenius activation energy (E_a), activation free energy change (ΔG^*), activation enthalpy change (ΔH^*), and activation entropy change (ΔS^*) can be calculated by using the following equations [55]:

$$\ln k_2 = \ln A - \frac{E_a}{RT} \quad (6)$$

$$\ln k_2 = \frac{k_B T K*}{h} \quad (7)$$

$$\Delta G* = -RT \ln K* \quad (8)$$

$$\Delta H* = E_a - RT \quad (9)$$

$$\Delta S* = \frac{\Delta H* - \Delta G*}{T} \quad (10)$$

where A is the Arrhenius factor, k_B and h are Boltzmann's constant (1.38×10^{-23} J/K) and Planck's constant (6.626×10^{-34} J s), R is the gas constant (8.3145 J/mol K), and K^* is the equilibrium constant at temperature T. A linear plot of $\ln k_2$ versus $1/T$ for the adsorption of MB onto the silica nano-sheets is constructed to generate the E_a value from the slope (Fig. 13). The E_a value was calculated to be 3.42 kJ/mol with a linear regression coefficient of 0.996. Thus, the values of ΔG^*, ΔH^*, and ΔS^* are 65.95 (71.63, 77.45) kJ/mol, 0.984 (0.776, 0.568) kJ/mol, and −0.222 (−0.223, −0.224) kJ/(K mol) at 20 (45, 70) °C, respectively.

The low ΔH^* values for the adsorption of MB with the silica nano-sheets give a clear evidence that the interactions between MB and the surface hydroxyl groups of the silica nano-sheets may be weak. On the other hand, the positive values of E_a,

Table 3
The desorption results

pH values	Desorption percentage (%)			
	H_2O/EtOH = 1:1	H_2O/EtOH = 1:3	H_2O/EtOH = 1:5	EtOH
1.5	30.24	31.85	34.82	44.26
5.5	29.49	30.11	32.47	43.35
9.0	28.13	28.50	30.11	41.74

ΔG^*, and ΔH^* indicate the presence of an energy barrier in the adsorption process. The positive values for these parameters are quite common because the activated complex in the transition state is in an excited form. The negative values of ΔS^* suggest decreased randomness at the solid/solution interface and no significant changes occur in the internal structure of the adsorbent through the adsorption of MB onto the silica nano-sheets.

3.5. Desorption

The adsorption capacity under the experiment was found to be 8.05 mg/g. The desorption ratio (%), the ratio of the weight of dye desorbed and the weight of dye adsorbed, of the MB-adsorbed silica nano-sheets with ethanol or water/ethanol solutions with certain v/v ratios at different pH values were given in Table 3. It showed that ethanol could be used for the regeneration of the silica nano-sheets and the higher acidity of ethanol favored the desorption.

4. Conclusions

The present study shows that the silica nano-sheets derived from vermiculite via acid leaching process are efficient adsorbent for the removal of cationic dye from aqueous solution.

(1) The maximum adsorption capacity was found to be 11.77 mg/g for MB.
(2) The adsorption of MB by the silica nano-sheets fits the Langmuir equilibrium isotherm perfectly.
(3) The kinetics of the cationic dye adsorption on the silica nano-sheets follows the pseudo-second-order model.
(4) And ethanol was found to be an efficient desorption agent for the dye adsorbed.

The silica nano-sheets are also expected to be used as substitute of porous silica gel for other molecules and ions.

References

[1] O. Ligrini, E. Oliveros, A. Braun, Photochemical processes for water treatment, Chem. Rev. 93 (1993) 671–698.
[2] H.S. Rai, M.S. Bhattacharyya, J. Singh, T.K. Bansal, P. Vats, U.C. Banerjee, Removal of dyes from the effluent of textile and dyestuff manufacturing industry: a review of emerging techniques with reference to biological treatment, Crit. Rev. Environ. Sci. Technol. 35 (2005) 219–238.
[3] C. Pelekani, V.L. Snoevink, Competitive adsorption between atrazine and methylene blue on activated carbon: the importance of pore size distribution, Carbon 38 (2003) 1423–1436.
[4] M.F.R. Pereira, S.F. Soares, J.J.M. Orfao, J.L. Fiqueiredo, Adsorption of dyes on activated carbons: influence of surface chemical groups, Carbon 41 (2003) 811–821.
[5] D.C.K. Ko, D.H.K. Tsang, J.F. Porter, G. McKay, Applications of multipore model for the mechanism identification during the adsorption of dye on activated carbon and bagasse pith, Langmuir 19 (2003) 722–730.
[6] M. Valix, W.H. Cheung, G. McKay, Roles of textural and surface chemical properties of activated carbon in adsorption of acid blue dye, Langmuir 22 (2006) 4574–4582.
[7] J.W. Lee, S.P. Choi, R. Thiruvenkatachari, W.G. Shim, H. Moon, Submerged microfiltration membrane coupled with alum coagulation/powdered activated carbon adsorption for complete decolorization of reactive dyes, Water Res. 40 (2006) 435–444.
[8] L.F. Vieira, M.J. Lemos, M.J. Reis, A.M. Botelho do Rego, UV–vis absorption, luminescence, and X-ray photoelectron spectroscopic studies of rhodamine dyes adsorbed onto different pore size silicas, Langmuir 16 (2000) 5673–5680.
[9] K.Y. Ho, G. McKay, K.L. Yeung, Selective adsorbents from ordered mesoporous silica, Langmuir 19 (2003) 3019–3024.
[10] A.G.S. Prado, B.S. Miranda, G.V.M. Guilherme, Interaction of indigo carmine dye with silica modified with humic acids at solid/liquid interface, Surf. Sci. 542 (2003) 276–282.
[11] Z. Yan, G.T. Li, L. Mu, S.Y. Tao, Pyridine-functionalized mesoporous silica as an efficient adsorbent for the removal of acid dyestuffs, J. Mater. Chem. 16 (2006) 1717–1725.
[12] P. Liu, L.X. Zhang, Adsorption of dyes from aqueous solutions or suspensions with clay nano-adsorbents, Sep. Purif. Technol. 58 (2007) 32–39.
[13] P. Liu, J.S. Guo, Polyacrylamide grafted attapulgite (PAM-ATP) via surface-initiated atom transfer radical polymerization (SI-ATRP) for removal of Hg(II) ion and dyes, Colloids Surf. A: Physicochem. Eng. Aspects 282–283 (2006) 498–503.
[14] A.F. Lopez, V. Martinez Martinez, J. Banuelos Prieto, I. Lopez Arbeloa, Adsorption of rhodamine 3B dye on saponite colloidal particles in aqueous suspensions, Langmuir 18 (2002) 2658–2664.
[15] M. Epstein, S. Yariv, Visible-spectroscopy study of the adsorption of alizarinate by Al-montmorillonite in aqueous suspensions and in solid state, J. Colloid Interface Sci. 263 (2003) 377–385.
[16] Y. Ozdemir, M. Doqan, M. Alkan, Adsorption of cationic dyes from aqueous solutions by sepiolite, Micropor. Mesopor. Mater. 96 (2006) 419–427.
[17] S.S. Tahir, N. Rauf, Removal of a cationic dye from aqueous solutions by adsorption onto bentonite clay, Chemosphere 63 (2006) 1842–1848.
[18] S.B. Wang, Z.H. Zhu, Characterisation and environmental application of an Australian natural zeolite for basic dye removal from aqueous solution, J. Hazard. Mater. 136 (2006) 946–952.
[19] Y.C. Wong, Y.S. Szeto, W.H. Cheung, G. McKay, Equilibrium studies for acid dye adsorption onto chitosan, Langmuir 19 (2003) 7888–7894.
[20] R.S. Blackburn, Natural polysaccharides and their interactions with dye molecules: applications in effluent treatment, Environ. Sci. Technol. 38 (2004) 4905–4909.
[21] S.B. Yamaki, D.S. Barros, C.M. Garcia, P. Socoloski, O.N. Pliveira Jr., T.D.Z. Atvars, Spectroscopic studies of the intermolecular interactions of congo red and tinopal CBS with modified cellulose fibers, Langmuir 21 (2005) 5414–5420.
[22] Z.G. Hu, J. Zhang, W.L. Chan, Y.S. Szeto, The sorption of acid dye onto chitosan nanoparticles, Polymer 47 (2006) 5838–5842.
[23] N.K. Lazaridis, G.Z. Kyzas, A.A. Vassiliou, D.N. Bikiaris, Chitosan derivatives as biosorbents for basic dyes, Langmuir 23 (2007) 7634–7643.
[24] C. Long, Z.Y. Lu, A.M. Li, W. Liu, Z.M. Jiang, J.L. Chen, G.X. Zhang, Adsorption of reactive dyes onto polymeric adsorbents: effect of pore structure and surface chemistry group of adsorbent on adsorptive properties, Sep. Purif. Technol. 44 (2005) 115–120.
[25] V. Bekiari, P. Lianos, Ureasil gels as a highly efficient adsorbent for water purification, Chem. Mater. 18 (2006) 4142–4146.
[26] A.V. Maffei, P.M. Budd, N.B. McKeown, Adsorption studies of a microporous phthalocyanine network polymer, Langmuir 22 (2006) 4225–4229.
[27] G. Crini, H.N. Peindy, F. Gimbert, C. Robert, Removal of C.I. Basic Green 4 (malachite green) from aqueous solutions by adsorption using cyclodextrin-

based adsorbent: kinetic and equilibrium studies, Sep. Purif. Technol. 53 (2007) 97–110.
[28] T. Robinson, B. Chandran, P. Niqam, Removal of dyes from an artificial textile dye effluent by two agricultural waste residues, corncob and barley husk, Environ. Int. 28 (2002) 29–33.
[29] P. Thiravetyan, S. Netpradit, S. Towprayoon, Application of 'waste' metal hydroxide sludge for adsorption of azo reactive dyes, Water Res. 37 (2003) 763–772.
[30] J.P. Silva, S. Sousa, J. Rodriques, H. Antunes, J.J. Porter, I. Goncalves, S. Ferreira-Dias, Adsorption of acid orange 7 dye in aqueous solutions by spent brewery grains, Sep. Purif. Technol. 40 (2004) 309–315.
[31] A. Mittal, L. Krishnan, V.K. Gupta, Removal and recovery of malachite green from wastewater using an agricultural waste material, de-oiled soya, Sep. Purif. Technol. 43 (2005) 125–133.
[32] R.C. Wu, J.H. Qu, Y.S. Chen, Magnetic powder MnO–Fe_2O_3 composite—a novel material for the removal of azo-dye from water, Water Res. 39 (2005) 630–638.
[33] Q.H. Hu, Z.P. Xu, S.Z. Qiao, F. Haghseresht, M. Wilson, G.Q. Lu, A novel color removal adsorbent from heterocoagulation of cationic and anionic clays, J. Colloid Interface Sci. 308 (2007) 191–199.
[34] E. Geraud, M. Bouhent, Z. Derriche, F. Leroux, V. Prevot, Texture effect of layered double hydroxides on chemisorption of Orange II, J. Phys. Chem. Solids 68 (2007) 818–823.
[35] S.B. Wang, H.T. Li, L.Y. Xu, Application of zeolite MCM-22 for basic dye removal from wastewater, J. Colloid Interface Sci. 295 (2006) 71–78.
[36] L.C. Juang, C.C. Wang, C.K. Lee, Adsorption of basic dyes onto MCM-41, Chemosphere 64 (2006) 1920–1928.
[37] B. Fugestu, S. Satoh, T. Shiba, T. Mizutani, Y.B. Lin, N. Terui, Y. Nodasaka, K. Sasa, K. Shimizu, T. Akasaka, M. Shindoh, K.I. Shibata, A. Yokoyama, M. Mori, K. Tanaka, Y. Sato, K. Tohji, S. Tanaka, N. Nishi, F. Watari, Caged multiwalled carbon nanotubes as the adsorbents for affinity-based elimination of ionic dyes, Environ. Sci. Technol. 38 (2004) 6890–6896.
[38] C.K. Lee, K.S. Lin, C.F. Wu, M.D. Lyu, C.C. Lo, Effects of synthesis temperature on the microstructures and basic dyes adsorption of titanate nanotubes, J. Hazard. Mater. 150 (2008) 494–503.
[39] M.F. Zhao, P. Liu, Adsorption behavior of methylene blue on halloysite nanotubes, Micropor. Mesopor. Mater., in press.
[40] S. Chakrabarti, B.K. Dutta, On the adsorption and diffusion of methylene blue in glass fibers, J. Colloid Interface Sci. 286 (2005) 807–811.
[41] A. Asok, M. Bandyopadhyay, A. Pal, Removal of crystal violet dye from wastewater by surfactant-modified alumina, Sep. Purif. Technol. 44 (2005) 139–144.
[42] M.A. Ibrahim, B.G. Lee, N.G. Park, Synthesis of new oligothiophene derivatives and their intercalation compounds: orientation effects, Synth. Met. 105 (1999) 35–42.
[43] H.R. Rittler, Method of treating phyllosilicates, U.S. Patent 4,952,388 (1990).
[44] J. Temuujin, K. Okada, K.J.D. MacKenzie, Preparation of porous silica from vermiculite by selective leaching, Appl. Clay Sci. 22 (2003) 187–195.
[45] M.C. Jimenez de Haro, J.L. Perez-Rodriguez, J. Poyato, L.A. Perez-Maqueda, V. Ramirez-Valle, A. Justo, A. Lerf, F.E. Wagner, Effect of ultrasound on preparation of porous materials from vermiculite, Appl. Clay Sci. 30 (2005) 11–20.
[46] C. Maqueda, A.S. Romero, E. Morillo, J.L. Perez-Rodriguez, Effect of grinding on the preparation of porous materials by acid-leached vermiculite, J. Phys. Chem. Solids 68 (2007) 1220–1224.
[47] M. Alkan, O. Demirbas, M. Dogan, Adsorption kinetics and thermodynamics of an anionic dye onto sepiolite, Micropor. Mesopor. Mater. 101 (2007) 388–396.
[48] M. Dogan, M. Alkan, Adsorption kinetics of methyl violet onto perlite, Chemosphere 50 (2003) 517–528.
[49] S.C. Tjong, Y.Z. Meng, A.S. Hay, Novel preparation and properties of polypropylene-vermiculite nanocomposites, Chem. Mater. 14 (2002) 44–51.
[50] X.S. Du, M. Xiao, Y.Z. Meng, T.F. Hung, A.V. Rajulu, S.C. Tjong, Synthesis of poly(arylene disulfide)-vermiculite nanocomposites via in situ ring-opening reaction of cyclic oligomers, Eur. Polym. J. 39 (2003) 1735–1739.
[51] J.M. Yeh, S.J. Liou, C.Y. Lai, P.C. Wu, T.Y. Tsai, Enhancement of corrosion protection effect in polyaniline via the formation of polyaniline-clay nanocomposite materials, Chem. Mater. 13 (2001) 1131–1136.
[52] Z. Shen, G.P. Simon, Y.B. Cheng, Comparison of solution intercalation and melt intercalation of polymer–clay nanocomposites, Polymer 43 (2002) 4251–4260.
[53] V.C. Taty-Costodes, H. Fauduet, C. Porte, A. Delacroixs, Removal of Cd(II) and Pb(II) ions, from aqueous solutions, by adsorption onto sawdust of *Pinus sylvestris*, J. Hazard. Mater. 105 (2003) 121–142.
[54] V. Vadivelan, K.V. Kumar, Equilibrium, kinetics, mechanism, and process design for the sorption of methylene blue onto rice husk, J. Colloid Interface Sci. 286 (2005) 90–100.
[55] M. Dogan, M. Alkan, A. Turkyılmaz, Y. Ozdemir, Kinetics and mechanism of removal of methylene blue by adsorption onto perlite, J. Hazard. Mater. B109 (2004) 141–148.